Thermodynamic Analysis of a Cascaded Latent Heat Store in a Pumped Thermal Electricity Storage System

Yao Zhao[1,2], Christos N. Markides[2] and Changying Zhao[1]

[1] Institute of Engineering Thermophysics, School of Mechanical Engineering, Shanghai Jiao Tong University, Shanghai (China)

[2] Clean Energy Processes (CEP) Laboratory, Department of Chemical Engineering, Imperial College London, London (United Kingdom)

Abstract

In this paper, the feasibility of replacing sensible-heat, packed-bed stores with cascaded latent-heat stores in pumped thermal electricity storage systems is explored through thermodynamic optimization based on exergy and entropy generation. The effects of the total stage number and of the *NTU* on the temperature distributions, energy, exergy and entropy generation in each stage, and over the cascaded store during the heat charging and discharging processes are discussed. The optimal outlet and melting temperatures of each stage during the heat charging process are both found to follow a geometric progression along the length of the store. It is found that the first few storage stages play a more important role in terms of overall heat transfer, exergy storage and release in both the heat charging and discharging processes. During the heat charging process, the total exergy storage rate increases and approaches its maximum, while the total entropy generation rate decreases and stabilizes as the total stage number and *NTU* increase. During the heat discharging process, the total heat transfer and total exergy release rates both increase as the total stage number and *NTU* increase, while the total entropy generation rate decreases. The highest roundtrip energy and exergy efficiencies are 94%-98% and 88%-95% for the investigated *NTU*s, respectively. The highest roundtrip energy and exergy efficiencies are 73%-98% and 60%-95% for the investigated total stage numbers.

Keywords: cascaded store, entropy generation, exergy, latent heat storage, pumped thermal electricity storage

1. Introduction

Renewable energy technologies are increasingly used for power generation, and with many of them having unpredictable (fluctuating and intermittent) generation characteristics, an increasing interest has grown in large-scale electrical energy storage solutions (Gür, 2018). Currently, three commercial large-scale electrical energy storage technologies are available at varying technology readiness levels (TRLs): pumped hydroelectric storage (PHS), compressed air energy storage (CAES) and flow batteries, all of which can offer power delivery rates over 1 MW and storage capacities over 1 MWh at the same time (Benato and Stoppato, 2018; Gür, 2018). However, PHS and CAES are both limited by geographical restrictions that arise from their operating principles and are key to their deployment, while flow batteries suffer from the poor lifetime and the high capital costs. Pumped thermal electricity storage (PTES) is regarded as a promising alternative large-scale electricity storage technology because it is neither subjected to geographical restrictions, nor subjected to lifetime and cost disadvantages in the way flow batteries are (Desrues et al., 2010). In PTES, excess electricity is used during charging to create a temperature difference between hot and cold stores. At a later time, when this is required, this temperature difference is used to drive a thermodynamic cycle to generate electricity during discharging, with a theoretical roundtrip efficiency of 100% (Steinmann, 2017).

In general, according to the selected thermodynamic cycle and working fluid, PTES technology can be divided into systems based on the Joule-Brayton cycle (Georgiou et al., 2018; McTigue et al., 2015; White et al., 2013), those based on the transcritical CO_2 cycle (Mercangöz et al., 2012; Morandin et al., 2012a, b; Morandin et al., 2013), and those based on the water-steam Rankine cycle (Jockenhöfer et al., 2018; Steinmann, 2017; Steinmann, 2014). In Joule-Brayton-cycle PTES systems, argon is often chosen as the working fluid and packed-bed tanks are recommended as the stores. White (2011) analysed the thermodynamic losses in the sensible-heat, packed-bed reservoirs of a PTES system and discussed their performance dependence on geometrical design parameters (e.g., pebble size) and operating conditions (e.g., temperatures). In a follow-up publication, White et al. (2014) further emphasized the links between wave propagation and thermodynamic losses in such sensible-heat packed-bed stores.

doi:10.18086/eurosun.2020.07.04 Available at http://proceedings.ises.org

However, packed-bed stores, and especially hot stores which operate at higher pressures, require high-strength materials to make the tanks withstand the pressures within the system, which increases their costs significantly. In this context, cascaded latent heat stores are an option for replacing packed-bed stores for the following reasons: (1) they alleviate the need for pressurized storage tanks; (2) they can have higher energy densities and smaller sizes; and (3) they have the potential to have lower costs if their smaller size can be exploited.

In this work, the feasibility of a cascaded latent-heat store as the hot store in a PTES system is explored from a thermodynamic perspective. The effects of the total stage number and *NTU* on the heat transfer, exergy storage/release and entropy generation rates in each stage and in the cascaded store are investigated during both the heat charging and discharging processes, and the resulting roundtrip energy and exergy efficiencies are reported.

2. Model description

2.1 Physical model

Figure 1 (a) shows a simplified PTES system layout with its four main components: a compressor, an expander and two thermal (hot and cold) stores. In this system, Joule-Brayton cycle and reverse Joule-Brayton cycle are used to realize the electricity charging and discharging processes. A Joule-Brayton cycle when using argon as the working fluid during charging is shown in the *T-s* diagram in Fig. 1 (b), which consists of a compression process (4→1), an expansion process (2→3) and two heat transfer processes (hot storage: 1→2, and cold storage: 3→4). The operating conditions during charging, along with relevant thermophysical properties are listed in Table 1.

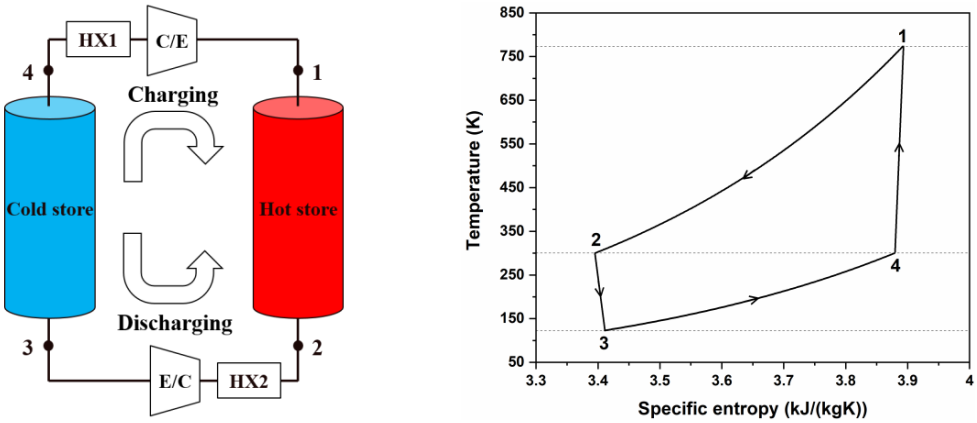

(a) Layout of a PTES system **(b) *T-s* diagram of a typical cycle during charging**

Fig. 1: Pumped thermal electricity storage: (a) Layout, and (b) thermodynamic cycle

Tab. 1: Operation conditions and thermophysical properties

Parameter	Unit	Value
Inlet temperature of hot store/outlet temperature of compressor, T_1	K	773
Outlet temperature of hot store/inlet temperature of expander, T_2	K	300
Inlet temperature of cold store/outlet temperature of expander, T_3	K	123
Outlet temperature of cold store/inlet temperature of compressor, T_4	K	300
Pressure in hot store, p_1 and p_2	bar	10
Pressure in cold store, p_3 and p_4	bar	1
Environmental temperature, T_e	K	293.15
Mass flow rate of argon, $\dot{m}$	kg/s	12.5
Specific heat capacity of argon, c_p	J/(kg K)	524.4

A cascaded latent-heat store used as the hot store in a PTES system is considered in this work, as shown in Fig. 2. Multiple phase change materials (PCMs) are used in this store, which are arranged according to their melting temperatures along the length of the store. A heat transfer fluid flows through the PCMs in order to perform the heat storage and release processes. In Fig. 2, $T_{m,i}$, $T_{c,i}$ and $T_{d,n-i+1}$ are the melting temperature and the HTF outlet temperatures in the i^{th} store/stage during charging and discharging, respectively. Some assumptions are made in order to simplify the physical problem: (1) temperature difference inside PCMs is neglected; (2) sensible heat of PCMs is also neglected compare with latent heat; (3) temperature distribution in the direction normal to the flow direction is neglected; (4) thermophysical properties of PCMs and HTF are constant; and (5) $T_{m,i} \geq T_e$; (6) $Q_{c,i} \geq Q_{d,i}$. Here, the HTF inlet and outlet temperatures during heat charging are fixed at 773 K and 300 K, respectively. The HTF inlet temperature during heat discharging is 293.15 K, which is equal to the environmental temperature.

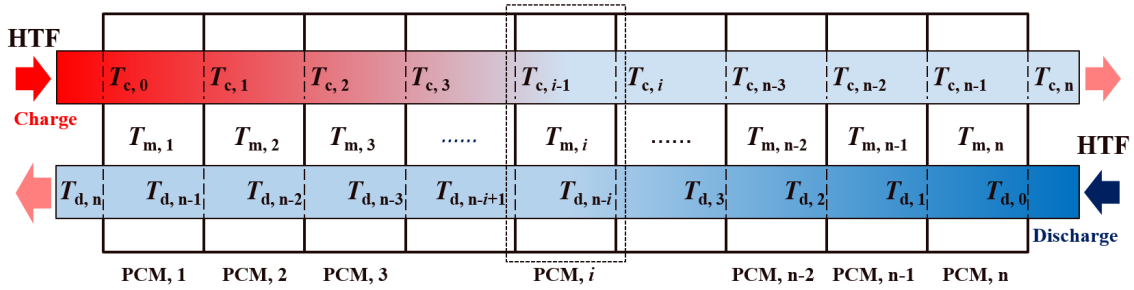

Fig. 2: Schematic diagram of a cascaded latent-heat store

2.2 Mathematical model

In the i^{th} stage during the heat charging process, the heat transfer rate is:

$$\dot{Q}_{c,i} = c_p \dot{m}\left(T_{c,i-1} - T_{c,i}\right) = U_i A_i \left\{\left(T_{c,i-1} - T_{c,i}\right) / \ln\left[\left(T_{c,i-1} - T_{m,i}\right) / \left(T_{c,i} - T_{m,i}\right)\right]\right\} \quad \text{(eq. 1)}$$

where U_i and A_i are the heat transfer coefficient and the heat exchange area, respectively.

The *NTU* in the i^{th} stage is defined as:

$$NTU = \left(U_i A_i\right) / \left(c_p \dot{m}\right) = \ln\left[\left(T_{c,i-1} - T_{m,i}\right) / \left(T_{c,i} - T_{m,i}\right)\right] \quad \text{(eq. 2)}$$

Then the melting temperature in the i^{th} stage can be obtained:

$$T_{m,i} = \left(C_i T_{c,i} - T_{c,i-1}\right) / \left(C_i - 1\right) \quad \text{(eq. 3)}$$

where $C_i = e^{NTU}$. To simplify the problem, the *NTU* in each stage is considered to be equal, so $C_i = C$.

The exergy storage rate can be calculated as:

$$\dot{E}x_{c,i} = \dot{Q}_{c,i}\left(1 - T_e / T_{m,i}\right) \quad \text{(eq. 4)}$$

The entropy generation rate can be expressed as:

$$\dot{S}_{g,c,i} = \Delta\dot{S}_{c,i} - \dot{S}_{f,c,i} - \left(s_{c,i-1} - s_{c,i}\right)\dot{m} = c_p \dot{m}\left[\ln\left(T_{c,i} / T_{c,i-1}\right) + \left(T_{c,i-1} - T_{c,i}\right) / T_{m,i}\right] \quad \text{(eq. 5)}$$

where $\Delta\dot{S}_{c,i}$ is the entropy accumulation rate, $\dot{S}_{f,c,i}$ the entropy transfer rate, and $s_{c,i-1}$ and $s_{c,i}$ the specific entropy at the inlet and outlet.

For the cascaded latent heat store, the total exergy storage and total entropy generation rate during the heat charging process are given as:

$$\dot{E}x_{c,total} = \sum_{i=1}^{n} \dot{E}x_{c,i} = \sum_{i=1}^{n}\left[\dot{Q}_{c,i}\left(1 - T_e / T_{m,i}\right)\right] \quad \text{(eq. 6)}$$

$$\dot{S}_{g,c,total} = \sum_{i=1}^{n} \dot{S}_{g,c,i} = c_p \dot{m} \sum_{i=1}^{n}\left[\ln\left(T_{c,i} / T_{c,i-1}\right) + \left(T_{c,i-1} - T_{c,i}\right) / T_{m,i}\right] \quad \text{(eq. 7)}$$

Thermodynamic optimization is performed based on the maximization of total exergy storage rate and the minimization of total entropy generation rate, respectively.

First, to maximize the total exergy storage rate, the following expressions should be satisfied:

$$\frac{\partial \dot{E}x_{\mathrm{c,total}}}{\partial T_{\mathrm{c},i}}=\begin{cases} c_{\mathrm{p}}\dot{m}T_{\mathrm{e}}\left(C-1\right)^{2}\left[T_{\mathrm{c},i\text{-}1}\Big/\left(CT_{\mathrm{c},i}-T_{\mathrm{c},i\text{-}1}\right)^{2}-T_{\mathrm{c},i+1}\Big/\left(CT_{\mathrm{c},i+1}-T_{\mathrm{c},i}\right)^{2}\right]=0, & 1\le i\le \mathrm{n\text{-}1} \\ c_{\mathrm{p}}\dot{m}\left[\left(C-1\right)^{2}T_{\mathrm{e}}T_{\mathrm{c,n\text{-}1}}\Big/\left(CT_{\mathrm{c,n}}-T_{\mathrm{c,n\text{-}1}}\right)^{2}-1\right]=0, & i=\mathrm{n} \end{cases} \quad \text{(eq. 8)}$$

$$\frac{\partial^{2}\dot{E}x_{\mathrm{c,total}}}{\partial T_{\mathrm{c},i}^{\ 2}}<0 \quad \text{(eq. 9)}$$

Second, the minimization of the total entropy generation rate must be carried out using the total heat transfer rate θ as a constraint. A new function is established based on the Lagrange multiplier method as shown below:

$$G\left(T_{\mathrm{c},1},T_{\mathrm{c},2},\cdots T_{\mathrm{c},i}\cdots,T_{\mathrm{c,n\text{-}1}},T_{\mathrm{c,n}},\delta\right)=\dot{S}_{\mathrm{g,c,total}}+\delta\left(\dot{Q}_{\mathrm{c,total}}-\theta\right) \quad \text{(eq. 10)}$$

The following relations should be satisfied:

$$\frac{\partial G}{\partial T_{\mathrm{c},i}}=\begin{cases} c_{\mathrm{p}}\dot{m}\left(C-1\right)^{2}\left[-T_{\mathrm{c},i\text{-}1}\Big/\left(CT_{\mathrm{c},i}-T_{\mathrm{c},i\text{-}1}\right)^{2}+T_{\mathrm{c},i+1}\Big/\left(CT_{\mathrm{c},i+1}-T_{\mathrm{c},i}\right)^{2}\right]=0, & 1\le i\le \mathrm{n\text{-}1} \\ c_{\mathrm{p}}\dot{m}\left[1/T_{\mathrm{c},i}-\left(C-1\right)^{2}T_{\mathrm{c},i\text{-}1}\Big/\left(CT_{\mathrm{c},i}-T_{\mathrm{c},i\text{-}1}\right)^{2}-\delta\right]=0, & i=\mathrm{n} \end{cases} \quad \text{(eq. 11)}$$

$$\frac{\partial G}{\partial \delta}=c_{\mathrm{p}}\dot{m}\left(T_{\mathrm{c},0}-T_{\mathrm{c,n}}\right)-\theta=0 \quad \text{(eq. 12)}$$

$$\frac{\partial^{2}G}{\partial T_{\mathrm{c},i}^{\ 2}}>0 \quad \text{(eq. 13)}$$

$$\frac{\partial^{2}G}{\partial \delta^{2}}>0 \quad \text{(eq. 14)}$$

By solving eqs. 8-9 and eqs. 11-14, the same analytical solution to the outlet temperature of the i^{th} stage during the heat charging process, $T_{\mathrm{c},i}$, exists for the above two optimization problems based on exergy and entropy generation:

$$T_{\mathrm{c},i,\mathrm{opt}}=T_{\mathrm{c},0}\left(T_{\mathrm{c,n,opt}}/T_{\mathrm{c},0}\right)^{i/\mathrm{n}}=T_{\mathrm{c},0}\left[1-\theta\Big/\left(c_{\mathrm{p}}\dot{m}T_{\mathrm{c},0}\right)\right]^{i/\mathrm{n}} \quad \text{(eq. 15)}$$

Eq. 15 shows that the optimal outlet temperatures of the stages are in a geometric progression, which means the following relations are satisfied:

$$T_{\mathrm{c,n,opt}}/T_{\mathrm{c,n\text{-}1,opt}}=T_{\mathrm{c,n\text{-}1,opt}}/T_{\mathrm{c,n\text{-}2,opt}}=\cdots=T_{\mathrm{c},i,\mathrm{opt}}/T_{\mathrm{c},i\text{-}1,\mathrm{opt}}=\cdots=T_{\mathrm{c},2,\mathrm{opt}}/T_{\mathrm{c},1,\mathrm{opt}}=T_{\mathrm{c},1,\mathrm{opt}}/T_{\mathrm{c},0}=q, \quad 1\le i\le \mathrm{n} \quad \text{(eq. 16)}$$

where q is the common ratio of the geometric progression. Then the optimal melting temperatures of the i^{th} stage are obtained together with eq. 3 as follows:

$$T_{\mathrm{m},i,\mathrm{opt}}=\left(CT_{\mathrm{c},i,\mathrm{opt}}-T_{\mathrm{c},i\text{-}1,\mathrm{opt}}\right)\Big/\left(C-1\right)=\left(CT_{\mathrm{c},0}q^{i}-T_{\mathrm{c},0}q^{i-1}\right)\Big/\left(C-1\right)=T_{\mathrm{c},0}q^{i-1}\left(Cq-1\right)/\left(C-1\right) \quad \text{(eq. 17)}$$

Eq. 17 shows that the optimal melting temperatures of the stages are also in a geometric progression with a common ratio of q.

In the heat discharging process, the melting temperature in each stage is the same with those of the heat charging process. For the i^{th} stage, the outlet temperature is calculated as:

$$T_{\mathrm{d,n}\text{-}i+1}=\frac{C-1}{C}T_{\mathrm{m},i,\mathrm{opt}}+\frac{1}{C}T_{\mathrm{d,n}\text{-}i}=\frac{C-1}{C}T_{\mathrm{m},i,\mathrm{opt}}+\sum_{j=2}^{\mathrm{n}\text{-}i+1}\frac{C-1}{C^{j}}T_{\mathrm{m},i+j\text{-}1,\mathrm{opt}}+\frac{1}{C^{\mathrm{n}\text{-}i+1}}T_{\mathrm{d},0} \quad \text{(eq. 18)}$$

The heat transfer rate, exergy release rate and entropy generation rate are written as:

$$\dot{Q}_{\mathrm{d},i}=c_{\mathrm{p}}\dot{m}\left(T_{\mathrm{d,n}\text{-}i+1}-T_{\mathrm{d,n}\text{-}i}\right) \quad \text{(eq. 19)}$$

$$\dot{E}x_{\mathrm{d},i}=c_{\mathrm{p}}\dot{m}\left[T_{\mathrm{d,n}\text{-}i+1}-T_{\mathrm{d,n}\text{-}i}-T_{\mathrm{e}}\ln\left(T_{\mathrm{d,n}\text{-}i+1}/T_{\mathrm{d,n}\text{-}i}\right)\right] \quad \text{(eq. 20)}$$

$$\dot{S}_{\mathrm{g,d},i}=c_{\mathrm{p}}\dot{m}\left[\left(T_{\mathrm{d,n}\text{-}i}-T_{\mathrm{d,n}\text{-}i+1}\right)\Big/T_{\mathrm{m},i}-\ln\left(T_{\mathrm{d,n}\text{-}i}/T_{\mathrm{d,n}\text{-}i+1}\right)\right] \quad \text{(eq. 21)}$$

Then the total heat transfer rate, total exergy release rate and total entropy generation rate are obtained:

$$\dot{Q}_{\mathrm{d,total}}=\sum_{i=1}^{\mathrm{n}}\dot{Q}_{\mathrm{d},i} \quad \text{(eq. 22)}$$

$$\dot{E}x_{\mathrm{d,total}} = \sum_{i=1}^{n} \dot{E}x_{\mathrm{d},i} \quad \text{(eq. 23)}$$

$$\dot{S}_{\mathrm{g,d,total}} = \sum_{i=1}^{n} \dot{S}_{\mathrm{g,d},i} \quad \text{(eq. 24)}$$

3. Results and discussion

3.1. Heat charging process

Figure 3 shows the melting/outlet temperatures, heat transfer rate, exergy storage rate and entropy generation rate in each stage when the total stage number is 4, 8 and 12, respectively, and *NTU* is 3. As shown in Fig. 3 (a), melting/outlet temperatures both decrease along the HTF flow direction. In Fig. 3 (b) and (c), both heat transfer rates and exergy storage rates also decrease along the HTF direction. The decreased heat transfer rate is caused by the smaller difference between melting temperatures and outlet temperatures in each stage. The smaller temperature difference, together with the lower melting temperature further makes the exergy storage rate decrease along the HTF flow direction. The stages close to the inlet play a more important role in heat transfer and exergy storage. The entropy generation rates in each stage are equal to each other, indicating the same thermodynamic irreversibility. As for the effect of total stage number, it is observed that larger total stage number could widen the range of melting/outlet temperatures, meaning more heat sources at different grades for the subsequent use. Larger total stage number could also cause the distribution of heat transfer rates and exergy storage rates in each stage to be more uniform, thus making full use of the heat storage capacity in each stage. The entropy generation rate in each stage tends to be lower for a larger total stage number.

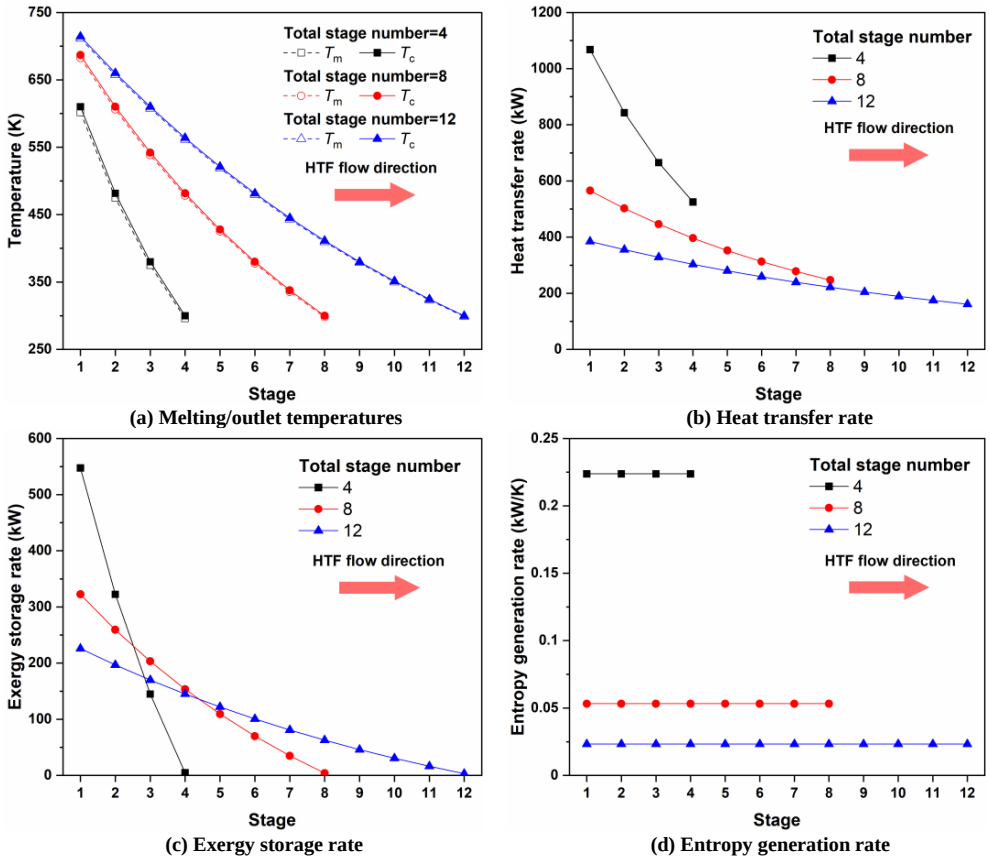

Fig. 3: Effect of total stage number on the thermodynamic performance in each stage

Figure 4 shows the effect of total stage number on the total exergy storage rate and total entropy generation rate of the latent heat store when *NTU* is 0.8, 1, 2, 3, 4 and 5, respectively. The total exergy transfer rate is 1.28 MW, as shown in Fig. 4 (a). As the total stage number increases, the total exergy storage rates increase and approach the total exergy transfer rate, indicating higher exergy storage efficiencies. When the total stage number increases to a critical number, the enhancement of exergy storage rate tends to be weaker, meaning that it is unnecessary to add more stages beyond the critical number from a thermodynamic view. The total entropy generation rates decrease and approach a certain

small value with the total stage number, indicating the thermodynamic irreversibility could be significantly reduced by adding certain stages. It is also shown that at *NTU*s of 0.8, 1, 2, 3 and 4, the thermodynamic parameters are neglected when the total stage number is smaller than certain value. If the heat transfer inside the stage is not strong enough, the optimal melting temperatures of the last few stages may be lower than the environmental temperature, especially for small total stage numbers, which causes the stored exergy not to be heat exergy.

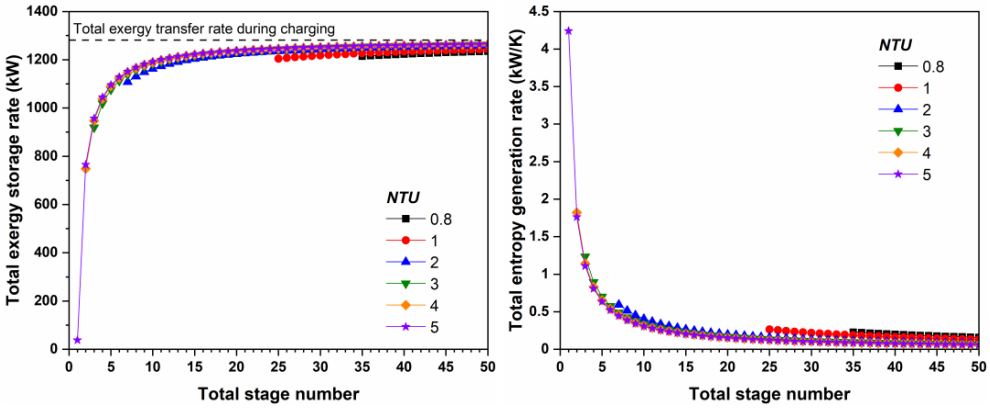

(a) Total exergy storage rate **(b) Total entropy generation rate**

Fig. 4: Effect of total stage number on the thermodynamic performance of the cascaded latent heat store

Figure 5 shows the melting/outlet temperatures, heat transfer rate, exergy storage rate and entropy generation rate in each stage when *NTU* is 1.2, 2.4 and 3.6, respectively and the total stage number is 20. For different *NTU*s, the outlet temperatures in each stage are the same due to the fixed inlet and outlet temperatures of the latent heat store, which further leads to the same heat transfer rates in each stage, as shown in Fig. 5 (a) and (b). As *NTU* increases, the melting temperatures in each stage tend to be raised and closer to the outlet temperature in each stage, because it is no longer necessary to maintain a large temperature difference for heat transfer. Then larger *NTU*s further improve the exergy storage rate and reduce the entropy generation rate in each stage, as shown in Fig. 5 (c) and (d).

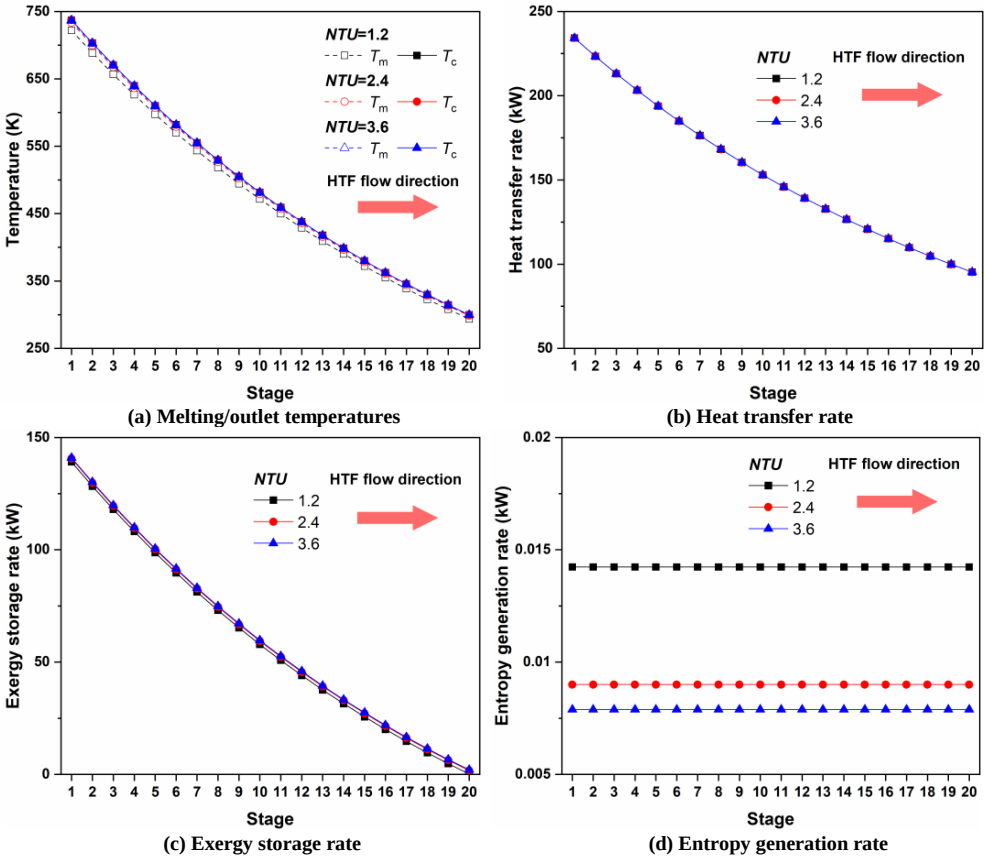

(a) Melting/outlet temperatures **(b) Heat transfer rate**

(c) Exergy storage rate **(d) Entropy generation rate**

Fig. 5: Effect of *NTU* on the thermodynamic performance in each stage

Figure 6 shows the effect of *NTU* on the total exergy storage rate and total entropy generation rate of the latent heat store when total storage number is 50, 40, 30, 20, 10 and 5, respectively. The total exergy transfer rate is also 1.28 MW. As *NTU* increases, the total exergy storage rates increase and then the enhancement effect tends to be weak, meaning that it is unnecessary to increase *NTU* beyond the critical number from a thermodynamic view. However, the maximum total exergy storage rates are raised for larger total stage numbers. The total entropy generation rates decrease and approach different certain small values with *NTU*, indicating the thermodynamic irreversibility could be significantly reduced by increasing *NTU*. It is shown that at low *NTU*s, the thermodynamic parameters are also neglected due to the optimal melting temperatures lower than the environmental temperature in the last few stages.

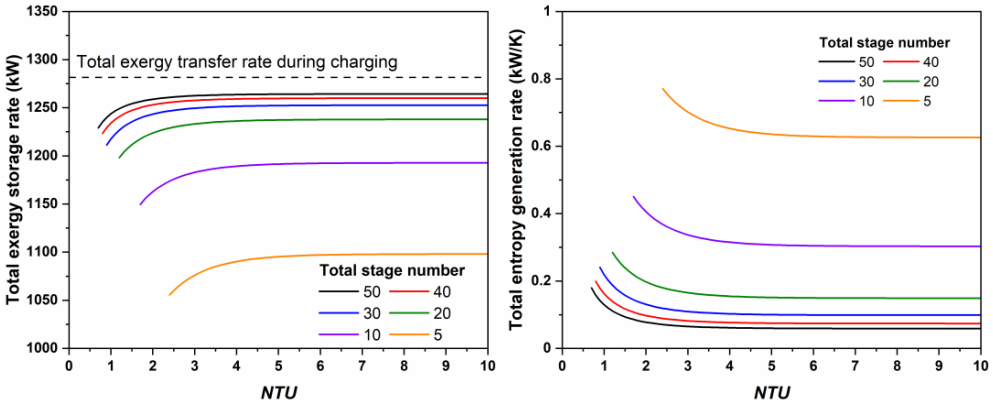

(a) Total exergy storage rate **(b) Total entropy generation rate**

Fig. 6: Effect of *NTU* on the thermodynamic performance of the cascaded latent heat store

3.2. Heat discharging process

Figure 7 shows the melting/outlet temperatures, heat transfer rate, exergy release rate and entropy generation rate in each stage when the total stage number is 4, 8 and 12, respectively, and *NTU* is 3. As shown in Fig. 7 (a), melting temperatures are the same with those of the heat charging process and outlet temperatures increase along the HTF flow direction. In Fig. 7 (b) and (c), both heat transfer rates and exergy release rates also increase along the HTF direction. The stages close to the inlet of the heat charging process also play a more important role in heat transfer and exergy release. Different from the heat charging process, entropy generation rates in each stage increase and then be stable, indicating the thermodynamic irreversibility in the last few stages is relatively low. As for the effect of total stage number, larger total stage numbers could significantly raise the outlet temperatures, meaning higher grades. Larger total stage number could also cause the distribution of heat transfer rates and exergy release rates in each stage to be more uniform. The entropy generation rates in the last few stages are affected by the HTF inlet temperature during discharging, but the average entropy generation rate in each stage tends to be lower for a larger total stage number.

Figure 8 shows the effect of total stage number on the total heat transfer rate, total exergy storage rate and total entropy generation rate of the latent heat store when *NTU* is 0.8, 1, 2, 3, 4 and 5, respectively. The total energy transfer rate and total exergy transfer rate during charging are 3.10 MW and 1.28 MW, respectively, as reference values. At *NTU*s of 0.8, 1, 2, 3 and 4, the thermodynamic parameters are neglected when the total stage number is smaller than certain value due to the corresponding melting temperatures lower than the environmental temperature. Moreover, considering the energy balance between the charging and discharging processes, the thermodynamic parameters in some last few stages are also neglected. As the total stage number increases, the total heat transfer rates and total exergy storage rates both increase. The highest roundtrip energy efficiencies are 94%, 95%, 97%, 98%, 98% and 98%, while the highest roundtrip exergy efficiencies reach 88%, 90%, 94%, 95%, 95% and 95% for *NTU*s of 0.8, 1, 2, 3, 4 and 5, respectively. The total entropy generation rates decrease with the total stage number, indicating the thermodynamic irreversibility could be significantly reduced by adding certain stages. When total stage number is 1, the entropy generation rate for *NTU* of 5 are close to zero due to the small differences between HTF temperatures and melting temperatures.

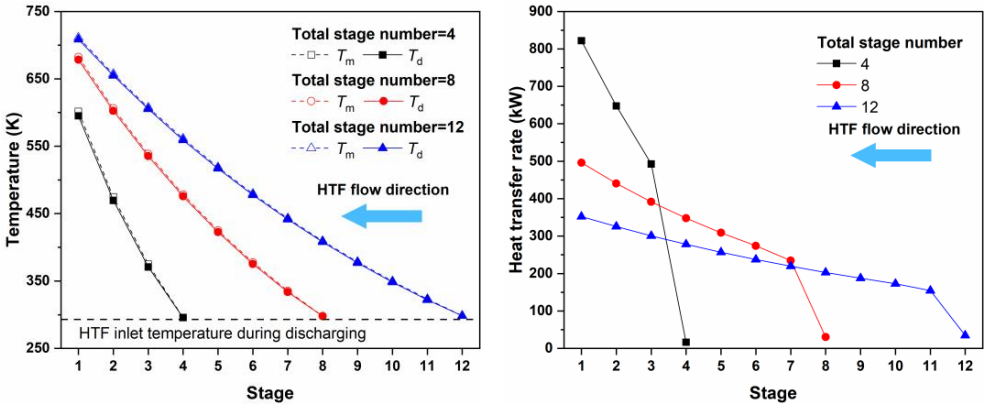

(a) Melting/outlet temperatures

(b) Heat transfer rate

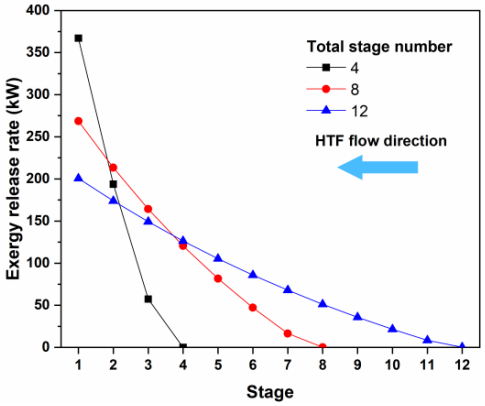

(c) Exergy release rate

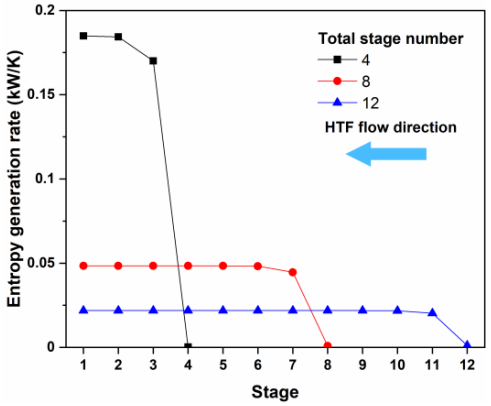

(d) Entropy generation rate

Fig. 7: Effect of total stage number on the thermodynamic performance in each stage

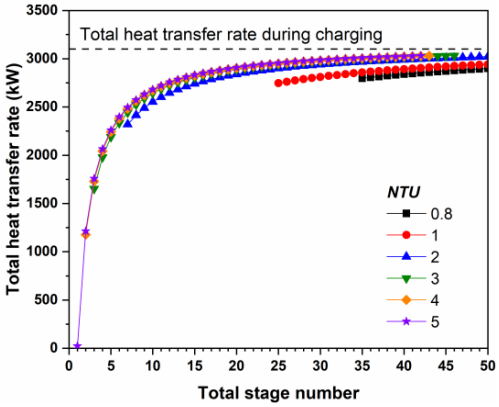

(a) Total heat transfer rate

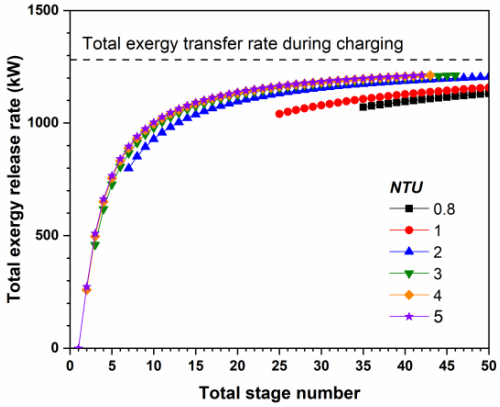

(b) Total exergy release rate

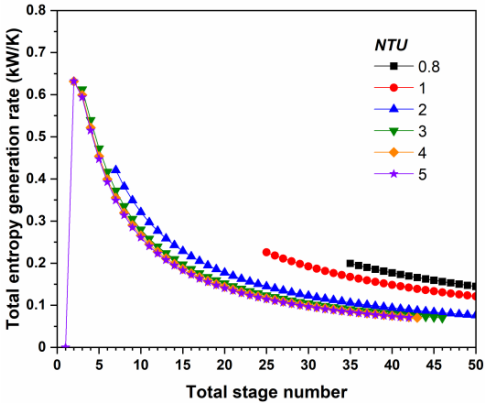

(c) Total entropy generation rate

Fig. 8: Effect of total stage number on the thermodynamic performance of the cascaded latent heat store

Figure 9 shows the melting/outlet temperatures, heat transfer rate, exergy release rate and entropy generation rate in each stage when *NTU* is 1.2, 2.4 and 3.6, respectively and the total stage number is 20. Melting temperatures are also the same with those of the heat charging process. As *NTU* increases, the outlet temperatures in each stage tend to be raised and closer to the melting temperatures in each stage. Larger *NTU*s further improve the heat transfer rate and exergy release rate in each stage. As for the entropy generation rate, the last few stages are also affected by the HTF inlet temperature during discharging, but the average entropy generation rate in each stage tends to be lower for a larger *NTU*.

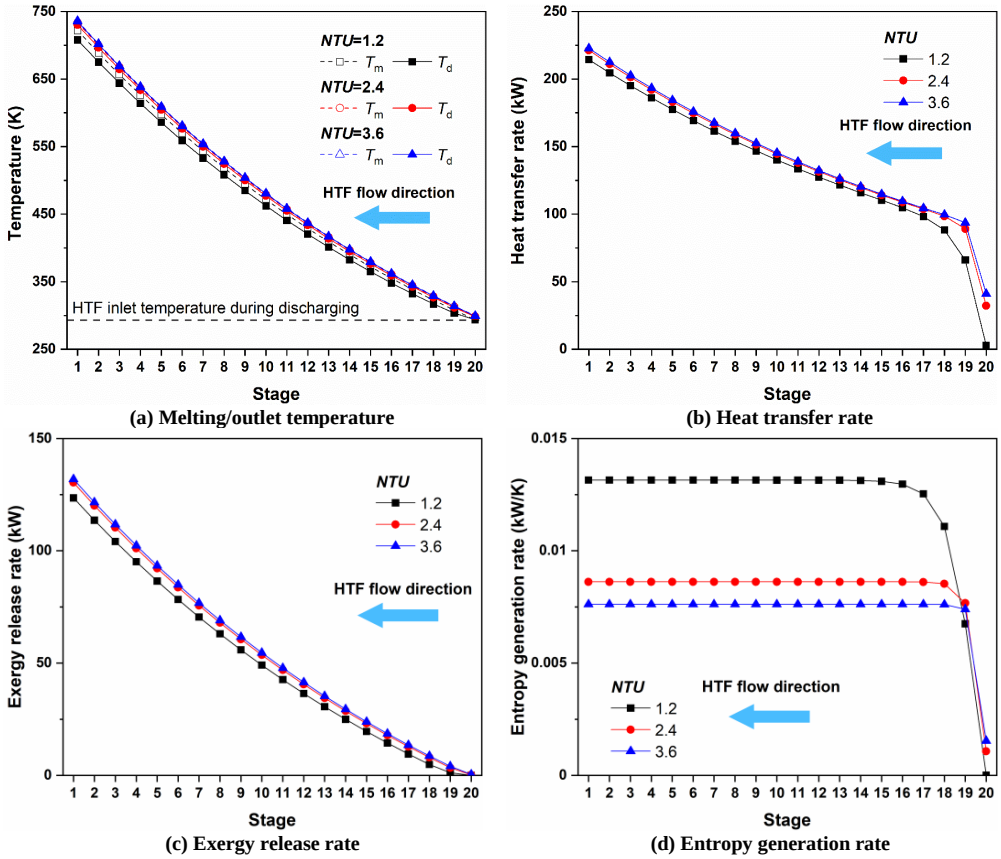

Fig. 9: Effect of *NTU* on the thermodynamic performance in each stage

Figure 10 shows the effect of the *NTU* on the total heat transfer rate, the total exergy storage rate and the total entropy generation rate of the latent heat store when total storage number is 50, 40, 30, 20, 10 and 5, respectively. The total energy transfer rate and total exergy transfer rate during charging are 3.10 MW and 1.28 MW, respectively, as reference values. For total stage number of 50, the total heat transfer rates and total exergy release rates increase with *NTU*, while for total stage number of 40, 30, 20, 10 and 5, the total heat transfer rates and total exergy release rates increase with *NTU* and then stabilize. The highest roundtrip energy efficiencies are 98%, 98%, 96%, 94%, 87% and 73%, while the highest roundtrip exergy efficiencies reach 95%, 94%, 92%, 89%, 79% and 60% for total stage numbers of 50, 40, 30, 20, 10 and 5, respectively. The total entropy generation rates decrease with *NTU*, indicating thermodynamic irreversibility could be significantly reduced by increasing *NTU*. For *NTU*s of 40, 30, 20, 10 and 5, the total entropy generation rates finally stabilize, meaning that thermodynamic irreversibility could not be further reduced beyond a certain *NTU*.

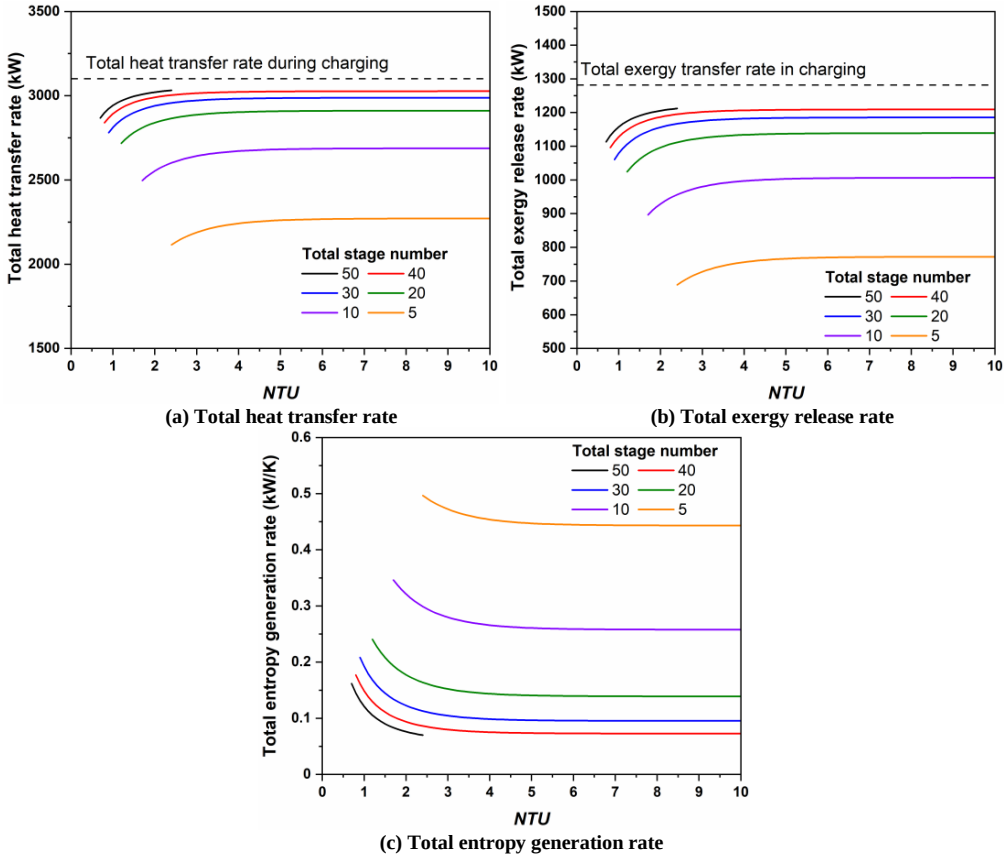

(a) Total heat transfer rate **(b) Total exergy release rate**

(c) Total entropy generation rate

Fig. 10: Effect of *NTU* on the thermodynamic performance of the cascaded latent heat store

4. Conclusions

The thermodynamic feasibility of cascaded latent-heat stores in pumped thermal electricity storage (PTES) systems was explored through exergy and entropy generation optimization. The effects of the total stage number and *NTU* on the temperature distributions, energy, exergy and entropy generation in each stage and over the cascaded store during heat charging and discharging were discussed.

The optimal outlet and melting temperatures in each stage during the heat charging process are found to follow a geometric progression along the length of the store. The first few storage stages play a more important role in heat transfer, exergy storage and release during both the heat charging and discharging processes.

A larger total stage number can widen the range of melting/outlet temperatures and cause the distribution of heat transfer rates and exergy storage/release rates in each stage to be more uniform. In the heat charging process, the entropy generation rate in each stage tends to be lower for a larger stage number, while in the heat discharging process, the entropy generation rates in the last few stages are affected by the HTF inlet temperature. In the heat charging process, the total exergy storage rate increases while the total entropy generation rate decreases as the total stage number increases up to a critical number, meaning that it is unnecessary to add more stages beyond the critical number from a thermodynamic perspective. In the heat discharging process, the total heat transfer rates and total exergy storage rates both increase, and the total entropy generation rates decrease as the total stage number increases. The highest roundtrip energy efficiencies range from 94% to 98%, while the highest roundtrip exergy efficiencies range from 88% to 95% for the presently investigated cases, respectively.

As the *NTU* increases, the outlet and melting temperatures in each stage tend to approach each other and the exergy storage/release rates are improved. In the heat discharging process, the heat transfer rates in each stage also increase with the *NTU*. In the heat charging process, the entropy generation rate in each stage tends to be lower for a larger *NTU*, while in the heat discharging process, the entropy generation rates in the last few stages are also affected by the HTF inlet temperature. In the heat charging process, the total exergy storage rates increase and the total entropy generation rates decrease as the *NTU* increases until a certain value. For fewer total stages, any enhancement of

the thermodynamic performance of the store by increasing the *NTU* decreases. In the discharging process, the total heat transfer rates and total exergy release rates increase, and the total entropy generation rates decrease with the *NTU*. The highest roundtrip energy efficiencies range from 73% to 98%, while the highest roundtrip exergy efficiencies range from 60% to 95% for the presently investigated cases, respectively.

5. Acknowledgments

This work was supported by the National Natural Science Foundation of China (Grant No. 51906150). It was also supported by the UK Engineering and Physical Sciences Research Council (EPSRC) [grant numbers EP/P004709/1, EP/R045518/1, and EP/S032622/1]. Data supporting this publication can be obtained on request from cep-lab@imperial.ac.uk.

6. References

Benato, A., Stoppato, A., 2018. Pumped Thermal Electricity Storage: A technology overview. Thermal Science and Engineering Progress 6, 301-315.

Desrues, T., Ruer, J., Marty, P., Fourmigué, J.F., 2010. A thermal energy storage process for large scale electric applications. Applied Thermal Engineering 30(5), 425-432.

Georgiou, S., Shah, N., Markides, C.N., 2018. A thermo-economic analysis and comparison of pumped-thermal and liquid-air electricity storage systems. Applied Energy 226, 1119-1133.

Gür, T.M., 2018. Review of electrical energy storage technologies, materials and systems: challenges and prospects for large-scale grid storage. Energy & Environmental Science 11(10), 2696-2767.

Jockenhöfer, H., Steinmann, W.-D., Bauer, D., 2018. Detailed numerical investigation of a pumped thermal energy storage with low temperature heat integration. Energy 145, 665-676.

McTigue, J.D., White, A.J., Markides, C.N., 2015. Parametric studies and optimisation of pumped thermal electricity storage. Applied Energy 137, 800-811.

Mercangöz, M., Hemrle, J., Kaufmann, L., Z'Graggen, A., Ohler, C., 2012. Electrothermal energy storage with transcritical CO2 cycles. Energy 45(1), 407-415.

Morandin, M., Maréchal, F., Mercangöz, M., Buchter, F., 2012a. Conceptual design of a thermo-electrical energy storage system based on heat integration of thermodynamic cycles – Part A: Methodology and base case. Energy 45(1), 375-385.

Morandin, M., Maréchal, F., Mercangöz, M., Buchter, F., 2012b. Conceptual design of a thermo-electrical energy storage system based on heat integration of thermodynamic cycles – Part B: Alternative system configurations. Energy 45(1), 386-396.

Morandin, M., Mercangöz, M., Hemrle, J., Maréchal, F., Favrat, D., 2013. Thermoeconomic design optimization of a thermo-electric energy storage system based on transcritical CO2 cycles. Energy 58, 571-587.

Steinmann, W.-D., 2017. Thermo-mechanical concepts for bulk energy storage. Renewable and Sustainable Energy Reviews 75, 205-219.

Steinmann, W.D., 2014. The CHEST (Compressed Heat Energy STorage) concept for facility scale thermo mechanical energy storage. Energy 69, 543-552.

White, A., McTigue, J., Markides, C., 2014. Wave propagation and thermodynamic losses in packed-bed thermal reservoirs for energy storage. Applied Energy 130, 648-657.

White, A., Parks, G., Markides, C.N., 2013. Thermodynamic analysis of pumped thermal electricity storage. Applied Thermal Engineering 53(2), 291-298.

White, A.J., 2011. Loss analysis of thermal reservoirs for electrical energy storage schemes. Applied Energy 88(11), 4150-4159.